Larhyss Journal, ISSN 1112-3680, n°61, March 2025, pp. 189-215

EXPERIMENTAL AND RESPONSE SURFACE METHODOLOGY-BASED OPTIMIZATION OF 3D-PRINTED IMPULSE TURBINE BUCKETS FOR SMALL HYDRO APPLICATIONS

***LAKDAWALA H.[1] *, PATEL V.[2], MODI D.[3]**, BAKHRU G.[4]*

[1] Assistant Professor, Mechanical Engineering Department, Dr. S. & S. S. Ghandhy Government Engineering College, Surat 395001, Gujarat, India
[2] Associate Professor, Mechanical Engineering Department, Sardar Vallabhbhai National Institute of Technology, Surat 395009, Gujarat, India
[3] Master of Engineering, Mechanical Engineering, Department of Mechanical Engineering, University of Windsor, Windsor, Ontario, Canada N9B 3P4
[4] Master of Engineering, Energy Engineering, Mechanical Engineering Department, Government Engineering College, Valsad 396001, Gujarat, India

(*) hnlgecs@gmail.com

Research Article – Available at http://larhyss.net/ojs/index.php/larhyss/index
Received July 27, 2024, Received in revised form February 25, 2025, Accepted February 27, 2025

ABSTRACT

Small hydro turbines have gained market traction due to the availability of water resources and lower installation costs. This study combines experimental and statistical approaches to optimize parameters influencing the displacement of impulse turbine buckets. Two Pelton turbine bucket designs, with size ratios of 0.67 (width: 31.83 mm) and 0.87 (width: 76 mm), were tested with three different jet diameters—8 mm, 10 mm, and 12 mm. The larger bucket exhibited a 30% increase in size compared to the smaller one. Both bucket types were fabricated using polylactic acid, a sustainable material, through 3D printing with fused deposition modeling. Response Surface Methodology (RSM), employing a Box-Behnken Design, was used to optimize the jet angle, jet diameter, and flow rate as numerical factors, while the bucket size ratio was treated as a categorical factor. These parameters were varied from the baseline design to assess their impact on bucket displacement. Experiments were conducted with different jet diameters at jet incidence angles of 90° ± 2.5°. Based on prior experimental investigations, the flow rate was adjusted within the range of 0.000068 to 0.000204 m³/s. Analysis of variance (ANOVA) revealed that flow rate is the most significant factor affecting bucket displacement, with a p-value less than 0.0001. The larger bucket (size ratio = 0.87) was more effective than the smaller one (size ratio =0.67) due to its ability to handle more water volume, reduce water diffusion, and create a higher moment arm. The quadratic model's optimal operating parameters were a nozzle angle of 90°, a jet diameter of 9 mm, and a flow rate of 0.001156 m³/s. The error between experimental results and RSM

predictions was 0.79%, indicating a strong correlation between these two. This study establishes the potential of using polylactic acid as a viable material for turbine buckets in small hydro applications, especially under varying operational conditions.

Keywords: 3-D printed turbine bucket, Jet diameter, Jet incidence, small hydro, Response Surface Methodology, Box Behnken Design

INTRODUCTION

Optimizing the dimensions and shape of Pelton turbine components has been a longstanding challenge, with the primary goal of improving overall turbine efficiency. The impact of several key parameters on power generation is considerable, as even minor variations can lead to significant changes in performance. As a result, numerous studies have been dedicated to refining bucket geometry and enhancing turbine performance, recognizing that the interplay between design elements, such as bucket curvature, jet impact angles, and surface area, plays a critical role in maximizing energy transfer and minimizing losses within the system. The bucket geometry optimization significantly affects the turbine's performance (Bhattarai et al., 2018). The jet dispersion and deviation significantly affect jet quality, thereby influencing Pelton turbine efficiency (Staubli et al., 2009).

The role of jet incidence angle and flow rate has also been a critical area of research. The pressure variations and jet velocity imbalances due to eccentricity. The pressure variation causes jet diffusion and hydraulic power loss, further impacting turbine performance (Jung et al., 2019). Nozzle misalignment with the bucket pitch circle leads to vibrations and damage, thus reducing operational efficiency and stability in Pelton turbines. The effect of jet angle on Turgo turbine performance was that the maximum power is generated at an intermediate jet incidence angle (Soe et al., 2019). The Pelton bucket found that the bucket power exhibits periodic changes when the relative position of the jet and bucket changes, and the most efficient energy conversion occurs when the jet is perpendicular to the bucket. The variable turbine head significantly impacts flow rate fluctuations, followed by variable injector opening and nozzle diameter (Nedelcu et al., 2021). So, the critical components of impulse turbines, including injector and spear design, are challenging. Increasing the discharge through the nozzle enhances Pelton turbine efficiency while increasing the nozzle diameter decreases it (Kholifah et al., 2018; Alomar et al., 2022). The nozzle-runner distance also affects the turbine performance. The water flows more axially when there is less distance between the nozzle outlet and the runner, while a greater distance results in more radial flow (Gupta et al., 2016). The secondary flow ratio effectively predicts free water jet deformation and can help mitigate jet deviation (Semlitsch, 2024). The multiphase flow in Pelton turbine buckets and optimizing flow dynamics increase renewable energy production (Suyesh et al., 2019).

Several studies have also explored the factors affecting runner torque and jet deformation. The outer region between the runner's pitch circle diameter and the cutout contributes most of the torque, with the Conda effect responsible for angular momentum and runner torque (Perrig et al., 2006). The design and configuration of turbine components,

particularly the number and positioning of buckets, have also been researched. The buckets' number, radial, and angular positions are interdependent, with efficiency improvements possible by reducing the number of buckets beyond a recommended limit (Židonis and Aggidis, 2016). The design for the Additive Manufacturing (DfAM) approach for producing Pelton turbine runners notably reduces the post-processing requirements for the turbine buckets after manufacturing. The optimum number of buckets is also essential for achieving maximum efficiency in Pelton turbines (Kim et al., 2017). A parametric model of a Pelton bucket reduces the time of torque calculation for the model runner, using the flow in only five rotating buckets numerically using the finite volume particle method (FVPM) (Vessaz et al., 2015). The turbine optimization was made faster and more cost-effective with improved runner, housing, and nozzle designs (Chitrakar et al., 2020).

The design of Pelton turbine buckets for micro-hydro applications has been identified as crucial. The Pico hydro Pelton turbine buckets can be designed and developed using locally sourced materials (Ebhota and Inambao, 2019). The 3D-printed Pelton turbine buckets have advantages in identifying design deficiencies and avoiding early-stage failures at a reduced cost. Regarding materials, the A390 cast aluminum alloy outperformed steel and plastic, providing optimal performance for the wheel and bucket without encountering unacceptable operating failure levels (Ishola et al., 2019). The feasibility analysis of coconut shell spoons as a bucket material showed promising results (Adanta et al., 2020). Several studies have explored turbine performance under varying conditions and experimentally investigated an Archimedes screw turbine, revealing non-linear efficiency behavior despite increases in power, torque, and angular velocity with increased flow rates (Zamani et al., 2023). The Turgo runner, compared to Pelton turbines, has a larger jet-to-runner diameter ratio and a higher specific speed for an impulse machine (Benzon et al., 2016). For pico-hydro impulse turbine buckets, the bucket curvature, cutout type, nozzle diameter ratio, bucket number, and runner diameter play a vital role in overall turbine performance, even buckets of unconventional material (Budiarso et al., 2018; Budiarso et al., 2019, Budiarso et al., 2020, Warjito et al., 2017 Warjito et al., 2018). The increase in bucket size by 15% and the increase in the angle of jet attack by 2 degrees increase the turbine efficiency (Alnakhlani et al., 2015). Meanwhile, the Pelton bucket has shown the possibility of increasing turbine efficiency by up to 4%, according to the available data from the "Illuchi N2" Hydroelectric Power Plant in Ecuador. Feasibility studies on micro-hydro systems have also yielded promising results. The micro hydro design, implementation, and analysis of Turgo turbines showed promising outcomes (Lajqi et al., 2021). A low static pressure head 2.5 m micro-Pelton turbine based on the water hammer phenomenon (Salah et al., 2003; Amara et al., 2013; Amara et al., 2016; Chaoui et al., 2016), operated effectively under a much lower head with the best efficiency (Elgammi and Hamad, 2022). Lastly, Pico-hydro technology is a promising solution for renewable energy production in developing countries, noting its cost-effectiveness, simplicity, and eco-friendliness.

In light of the aforementioned context, it is pertinent to underscore the critical importance of renewable energy sources. Renewable energy is essential for sustainable development, energy security, and environmental protection, offering a clean alternative to fossil fuels.

Hydropower, one of the most widely used renewable sources, provides stable and reliable electricity generation while supporting water resource management through reservoirs and flood control systems (Faye, 2016; Aroua, 2020; Hafnaoui et al., 2022; Hafnaoui et al., 2023; Remini, 2023; Zegait and Pizzo, 2023; Verma et al., 2023; Mehta et al., 2023; Shaikh et al., 2024). Hydrogen production, particularly green hydrogen derived from water electrolysis powered by renewables, represents a promising solution for decarbonizing industries, transportation, and energy storage. Other renewable sources, such as solar and wind energy, contribute to diversifying the global energy mix, reducing greenhouse gas emissions, and fostering economic resilience. By investing in innovative renewable energy technologies, countries can mitigate climate change, enhance energy independence, and promote long-term environmental sustainability. The following pertinent references are strongly recommended for readers seeking a deeper understanding of the crucial key aspects previously discussed (Boubou-Bouziani, 2015; Goran and Jelisavka, 2016; Belloufi et al., 2016; Debbache and Derfouf, 2018; Long et al., 2023; Ambaliya et al., 2024)

The use of Response Surface Methodology (RSM) has been identified as a valuable tool for the optimization of various turbine parameters. The RSM helps maximize energy extraction in Turgo impulse turbines (Gallego et al., 2021) and optimize the number of blades and hub-to-rotor diameter ratio, parameters that significantly impact the hydraulic performance of a siphon turbine (Guerra et al., 2024). Also, optimize the basin and inlet channel of gravitational water vortex hydraulic turbines (Velásquez et al., 2022) and design a 3D-printed Gravitational Vortex Turbine (GVT) runner (Betancour et al., 2023), with satisfactory results across a range of parameters. Apart from radial flow, RSM is also useful for the Design optimization of an Archimedes screw turbine axial flow turbine for hydrokinetic applications (Bouvant et al., 2021).

The sequence of processes carried out in the present study is charted in Fig. 1. The present study involves research gap identification from the available literature, design, and manufacturing buckets on the 3D printer for low-head small hydro application, experimentation for deciding the range of RSM designing of experiments and arriving at the optimum solution. The statistical methods also eliminate ineffective parameters if optimality is not reached and again recalculated with suggested readings.

This work introduces a novel approach using polylactic acid (PLA), a sustainable and biodegradable material, to design and study Pelton turbine impulse blades (buckets). While past studies focused mainly on metallic materials, this research pioneers using PLA, which has not been explored in turbine applications. Two bucket size ratios were manufactured using 3D printing to compare the performance of PLA-based buckets with traditional metallic ones. The study also investigates key parameters like jet angle, jet diameter, and bucket size ratio, particularly for low-head conditions. Optimization is achieved through experimental and statistical methods, employing Response Surface Methodology (RSM) with Box Behnken Design (BBD), a novel application in small hydro turbine research.

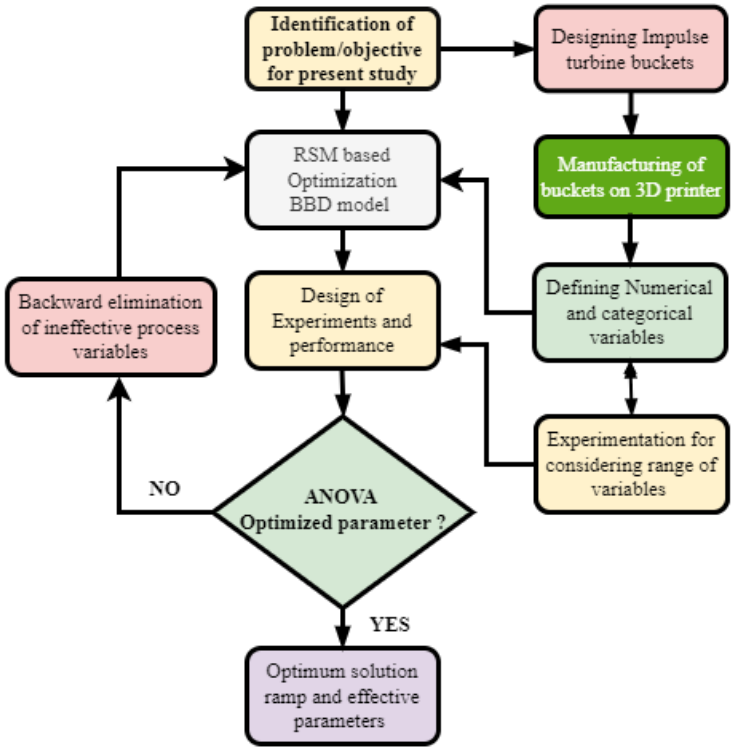

Figure 1: Flow diagram for the present study

EXPERIMENTAL SETUP

Fig. 2 presents the graphical setup of the test. The flow line includes 1-inch Polyvinyl Chloride (PVC) pipes for the bypass, delivery, suction lines, and fittings designed to handle substantial water flows. As shown in the schematic, an electric water pump, equipped with a centrifugal impeller, is positioned at the setup's lowest part to facilitate water flow, capable of delivering up to a 10-meter head through the discharge line. A rotameter, with a capacity range of 0.00005 to 0.00025 m^3/s, and a glass tube with a float measure the flow rate just above the discharge line. The protractor, graduated in 1-degree steps up to 180 degrees, measures the nozzle's angular position once clamped to the nozzle assembly.

A flexible hose connects the line to the main nozzle assembly, reducing piping length and fitting losses. The horizontal nozzle assembly, designed with inner threads, accommodates various brass nozzles. A transparent acrylic chamber allows front flow visualization, while a protractor measures jet deviation angles with a least count of 1 degree. Positioned before the nozzle, the hinged bucket assembly with an adjustable stand

holds various bucket sizes for testing. A dial indicator (0-10 mm, LC 0.01 mm) with a magnetic stand (MS, Yuzuki makes, magnetic force 80 kgf, fine adjustment screw, 8 mm clamp hole) is attached to the back of the bucket to measure water jet displacement. All the parameter-measuring instruments are arranged in-line in the setup. The flow line and nozzle details are mentioned in Table 1.

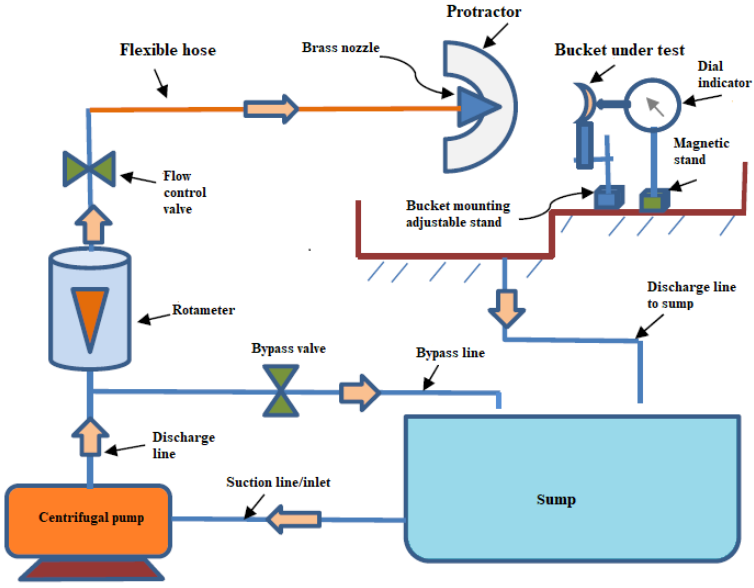

Figure 2: Schematic diagram of experimental setup

Table 1: Flow line and nozzle details

Description	Size
Delivery line size	1 inch
Rotameter discharge range (Q_r)	0.00005 - 0.00025 m^3/s
Jet diameter (d_j)	12 mm. 10 mm and 8 mm
Standoff distance from the nozzle to the bucket in each case (S_n)	150 mm
Test head (Ht)	9 m (Considering losses at pump and pipe)
Nozzle length (mm)	34, 32 and 30 mm
Height of adjustment possible on the mounting stand	220 mm
Dial indicator	Range 0-10 mm (LC 0.01 mm)

MATERIAL AND METHODOLOGY

Fig. 3 shows the arrangement made while performing experiments for different combinations of parameters considered for the present study. The bucket has been arranged against the water faucet in different jet angular positions and sizes to reveal the effect on bucket displacement.

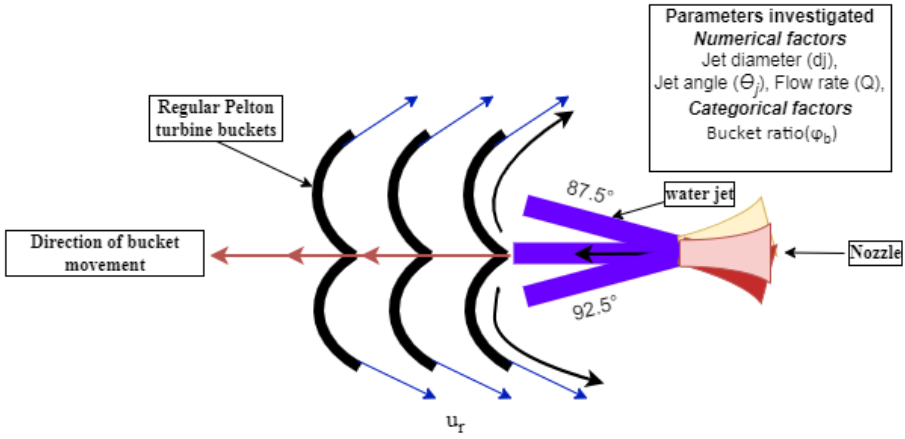

Figure 3: The graphical representation of parameters

The roughness value of manufactured buckets, the jet diameters, the angle of jet incidence on the buckets, and the bucket ratio are mentioned in Table 2. The horizontal distance between the bucket center and nozzle tip, i.e., the standoff distance of the nozzle (S_n) in each case, was kept constant at 150 mm for all the test runs. The surface roughness value was measured on the inner surface of the bucket with the Mitutoyo SJ-210 surface roughness tester.

Table 2: Buckets under investigation

Empirical formula for bucket design	Buckets	Jet diameter(d_j)	Angle of jet incidence (θ_j)	Roughness value (R_a)
Bucket depth (D_b) = (0.8-1.2) d_j Bucket width (B) = (2.4-4) d_j Bucket height (H) = (2.28-3.3) d_j Bucket offset (K) = (0.1-0.17) d_j Bucket notch (N_d) = (0-0.35) d_j	Larger bucket, $\emptyset_b$ = 0.87 Width (B) =76 mm	8,10,12 mm	90°±2.5°	14.230 µm
	Smaller bucket, $\emptyset_b$ = 0.67 Width (B) =31.83 mm	8,10,12 mm	90°±2.5°	14.072 µm

The experimental setup and all the instruments used for measuring parameters are illustrated in Fig. 4 of the present study. A short flexible hose connects the nozzle and the rotameter, allowing for accurate flow measurement. The nozzle is mounted on a protractor with graduated angles, enabling precise adjustments to the jet angle. This setup allows for the variation of the jet's angle of incidence on the turbine buckets, providing flexibility in examining the effects of non-normal jet impacts on performance.

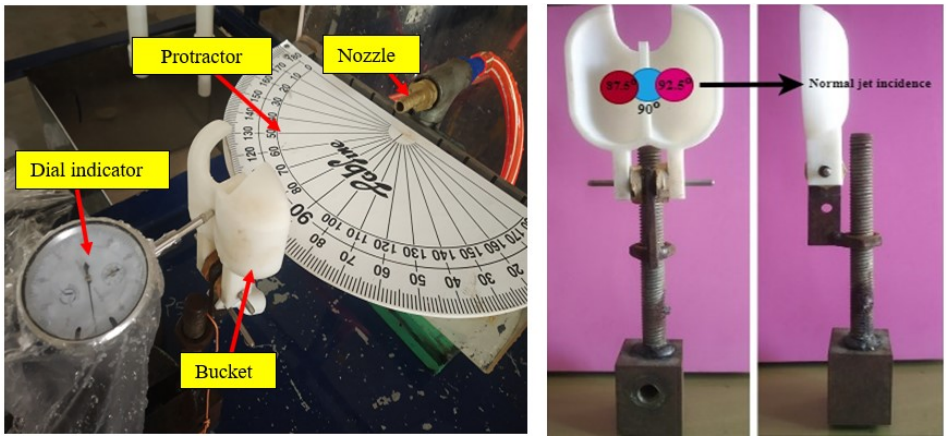

(a) **(b)**

Figure 4: (a) Experimental setup (b) Point of jet incidences on the bucket

DATA REDUCTION

The mass of fluid ($\dot{m}$) strikes the bucket with velocity (V) at the exit of the nozzle. The theoretical (u_{th}) and the initial velocity are mentioned in equations (1) and (2) possessed by the jet issued from the nozzle, respectively. The mass of fluid ($\dot{m}$) striking the bucket was measured with the rotameter. The movement of the bucket, which was assumed to be linear for a small distance of a larger rotational radius around the hinge, was measured with a dial gauge indicator attached to the frame. However, while calculating the normal force, the angular movement of the bucket was included. From the fundamental equations, the theoretical jet velocity can be given as follows (Gouryev et al., 2020; Amara and Achour, 2020):

$$u_{th} = C_V \sqrt{2\,g\,H}\,, m/s \tag{1}$$

Where C_v is the velocity coefficient assumed as unity, and H is the head available at the nozzle in meters

$$u = \frac{\dot{m}}{\rho\, A}\,, m/s \tag{2}$$

The force experienced by the bucket is the product of the mass flow rate of fluid ($\dot{m}$) and the relative velocity between the jet and bucket (u_r). The jet with high kinetic energy (KE_{jet}) strikes the bucket and causes the bucket to move in the direction of the jet. The

force exerted by the jet normally on the bucket is given by equation (3), assuming the bucket absorbs all the momentum of the water jet.

$$F_b = \dot{m} \times u_r \, , N \tag{3}$$

The work done (W.D) on the bucket is the product of torque exerted by the jet on the bucket (T_b) and corresponding angular bucket displacement ($\delta_{\theta b}$), and it is given by equation (4)

$$W.D = \; T_b \times \delta_{\theta b}, N - mm \tag{4}$$

Fig. 5 illustrates the relationship between the force exerted by the jet and bucket displacement for 8 mm, 10 mm, and 12 mm nozzles with variable flow rates. Jet angles other than normal result in less force due to jet deviation, often caused by faulty nozzle manufacturing, spear rod eccentricity, or clogged nozzles. Normal jet incidence is effective for both buckets, with the $\emptyset_b$ = 0.87 bucket displacing more than the $\emptyset_b$ = 0.67 bucket. The bifurcated water jet exits through the bucket's inner surface, and maximum normal force is observed with the $\emptyset_b$ = 0.87 buckets.

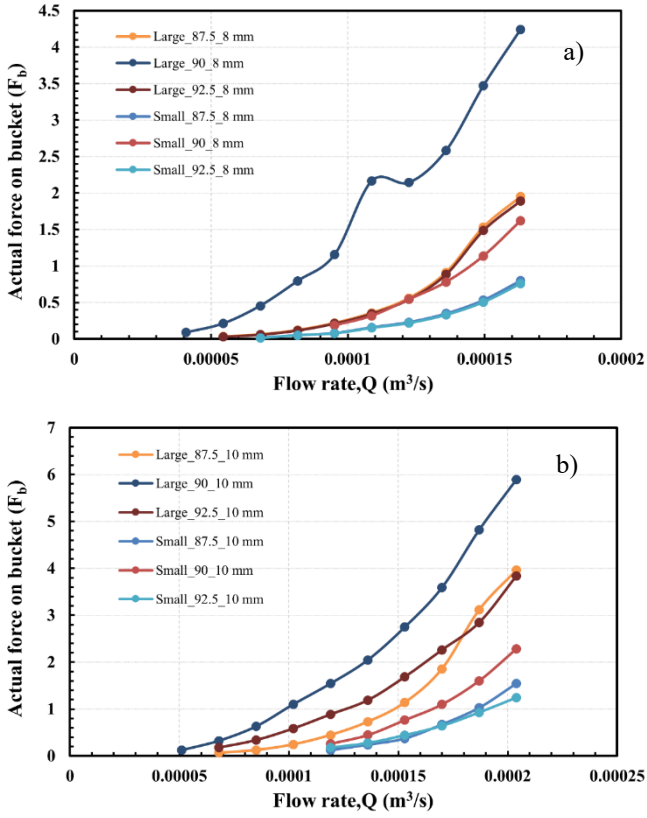

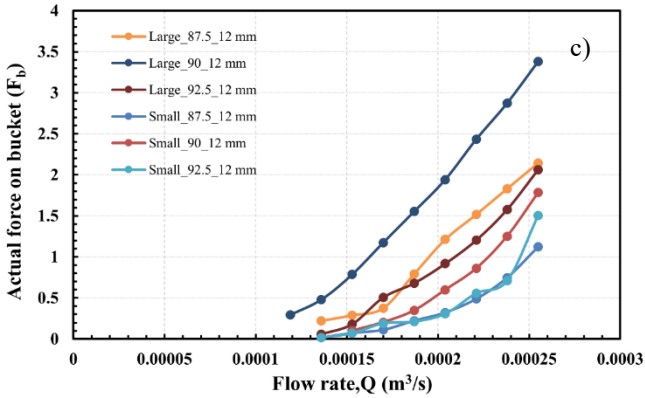

Figure 5: Actual force on the bucket (N) vs. Flowrate (m^3/s) for the buckets with (a) 8 mm, (b) 10 mm, and (c) 12 mm nozzles

A positive correlation between flow rate and displacement is exhibited by all curves, indicating that a proportional increase in displacement results from an increase in flow rate. It was observed that the 10 mm diameter nozzle continues to perform well with varying flow conditions. The inclination of the jet brings uneven bifurcation of the jet and unstable bucket movement. It has been observed that the diffusion in water at the jet striking point in the half-hemispherical part of the bucket is greater. Thus, diffusion has a detrimental effect on the bucket displacement observed in the present study, which aligns with the literature studied.

RESULTS AND DISCUSSION

Response Surface Methodology (RSM) for Maximum Force/Work Done on Bucket

RSM offers statistical and mathematical techniques derived from experimental models to fit the actual data associated with the experimental setting. Reducing the number of experiments runs and examining how the elements interact is utilized to optimize the intended factors. The response surface is depicted as a three-dimensional topological surface that delineates the relationship between the independent and dependent response variables. This graphical representation facilitates the identification of trends, patterns, and optimal operating conditions within the experimental design space (Box et al., 2005; Raymond et al., 2016).

Box-Behnken Designs (BBD) require fewer runs to obtain higher-order response surfaces than a standard factorial technique. The following expression, as stated in equation (5), can describe the system response (δ_b) and the set of factors (d_j, θ_j, Q).

$$\delta_b = f(d_j, \theta_j, Q) \tag{5}$$

The number of tests required to reveal the effect of the above factors is described by equation (6), as stated below.

$$N = n_c(2^n + 2n + n_r) \tag{6}$$

Where n_c is the number of categorical elements, and N is the number of needed runs. The number of replications is nr, while the number of numerical factors is n. So, for the present study, 3 numerical factors and 1 categorical factor are used as two buckets, and 3 replications are considered. Hence, it yields 34 runs as per the above calculations.

Table 3: Selected input parameters for optimization

Independent Parameter	Low (-1)	High (+1)	Coded value
Angle of a jet (θ_j), degrees	87.5°	92.5°	θ_j
Jet diameter (d_j), mm	8 mm	12 mm	d_j
Flow rate (Q), m^3/s	0.000068	0.000204	Q
Ratio of axial length to radial width of a bucket ($\emptyset_b$) (= Bucket size ratio)	0.67	0.87	$\emptyset_b$

As shown in Table 3 above, the selected independent variables with upper and lower investigation values are considered for the present study. Analysis was carried out using Design Expert 13.0 software and compared for adequacy and optimization of parameters. ANOVA is a statistical technique used to categorize the individual interaction of the contractors of the experimental design outcomes. Engineers and researchers can optimize the turbine design for better performance by identifying which factors significantly affect the output. The current study found that the bucket displacement follows the quadratic model and is effective compared to the linear model suggested by the software.

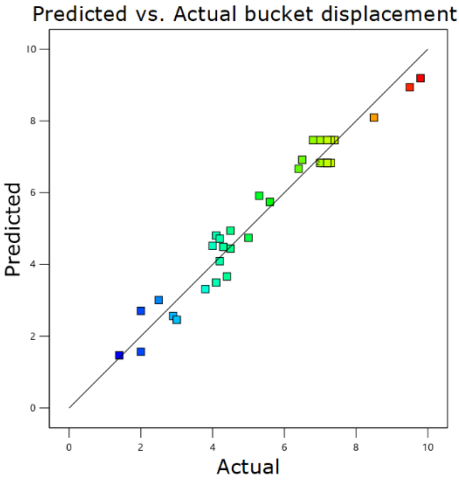

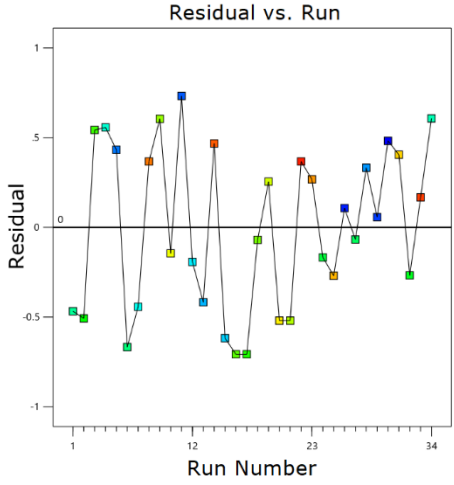

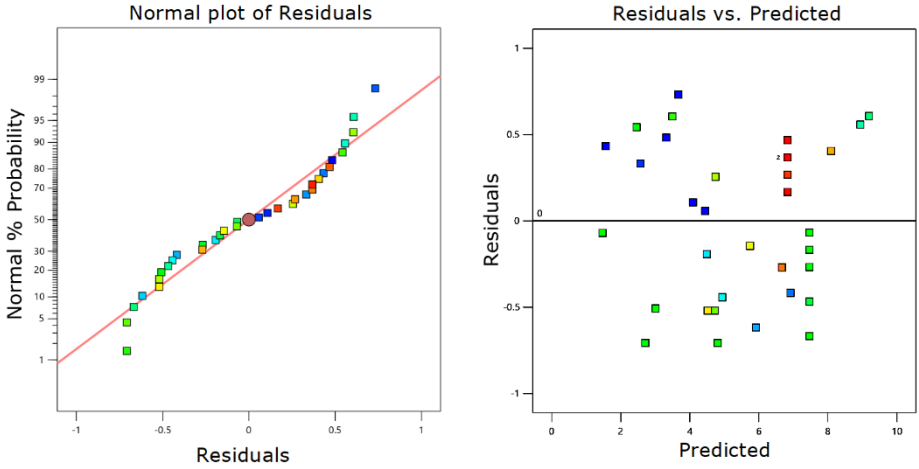

Figure 6: The charts for actual and predicted models for the BBD regression model

The graphs in Fig. 6 show that the experiments were performed randomly to reduce the errors and the effect of factors. The points' closeness to the diagonal line suggests that the estimates are accurate and that there aren't many differences from the actual measured values. The consistency across the range of values (0 to 10) further confirms the model's robustness in predicting bucket displacement accurately. It also depicts the experimental and predicted responses for the transformed (reduced) regression model mentioned in Table 4; the experiment was run in combination and carried out randomly. The metadata of the response surface is verified with experimental values.

Table 4: Design of Experiment (DoE) Box-Behnken Designs (BBD) matrix

Test Run	C.F ($\emptyset_b$)	Angle of the jet (θ_j), degree	Jet diameter (d_j), m*10^{-3}	Flow rate (Q),m^3/s *10^{-4}	Results for bucket displacement (δ_b), mm Regression model		
					Exp.	Pred.	Residual
1	0.67	90°	10	1.3	7.2	7.47	-0.4676
2	0.87	87.5°	8	1.3	4.1	3.01	-0.5074
3	0.87	87.5°	12	1.3	5.6	2.46	0.5426
4	0.67	90°	8	1.7	4.4	8.94	0.5574
5	0.67	87.5°	10	0.85	4.3	1.57	0.4324
6	0.67	90°	10	1.3	6.5	7.47	-0.6676
7	0.67	90°	12	0.85	7.3	4.94	-0.4426
8	0.87	90°	10	1.3	5.3	6.83	0.3676
9	0.87	92.5	10	0.85	2	3.49	0.6051
10	0.87	90°	8	0.85	4.1	5.74	-0.1449
11	0.67	92.5°	12	1.3	1.4	3.67	0.7324
12	0.67	90°	8	0.85	5	4.49	-0.1926
13	0.67	87.5°	10	1.7	4	6.92	-0.4176
14	0.87	90°	10	1.3	4.2	6.83	0.4676
15	0.67	92.5°	10	1.7	7.2	5.92	-0.6176

16	0.87	92.5°	12	1.3	7.1	2.71	-0.7074
17	0.87	92.5°	8	1.3	7.3	4.81	-0.7074
18	0.87	87.5°	10	0.85	6.4	1.47	-0.0699
19	0.87	92.5°	10	1.7	4.2	4.74	0.2551
20	0.87	90°	12	0.85	7.4	4.52	-0.5199
21	0.87	87.5°	10	1.7	2.9	4.72	-0.5199
22	0.87	90°	10	1.3	4.5	6.83	0.3676
23	0.87	90°	10	1.3	3.8	6.83	0.2676
24	0.67	90°	10	1.3	8.5	7.47	-0.1676
25	0.87	90°	12	1.7	7.2	6.67	-0.2699
26	0.67	92.5°	8	1.3	7	4.09	0.1074
27	0.67	90°	10	1.3	9.8	7.47	-0.0676
28	0.67	92.5°	10	0.85	7.2	2.57	0.3324
29	0.67	87.5°	12	1.3	4.1	4.44	0.0574
30	0.67	87.5°	8	1.3	5.6	3.32	0.4824
31	0.87	90°	8	1.7	4.4	8.09	0.4051
32	0.67	90°	10	1.3	4.3	7.47	-0.2676
33	0.87	90°	10	1.3	6.5	6.83	0.1676
34	0.67	90°	12	1.7	7.3	9.19	0.6074

Each test run was carried out using the combinations of parameters described by the software. The "Residual" variable represents the unexplained variation in the data. It provides a measurement of model fit quality. Residuals are generated from diverse sources like measurement error, unaccounted variables, or inherent randomness within the system being investigated. The coded Equation can be written under equation (7), which includes all the parameters.

$$\delta_b = 7.15 + 0.2562\theta_j - 0.24386d_j + 1.65Q - 0.3176\emptyset_b - 0.3875\theta_j d_j - 0.5\theta_j Q + 0.2563\theta_j \emptyset_b - 0.05 d_j Q - 0.4187 d_j \emptyset_b - 0.5250 Q \emptyset_b - 3.12\theta_j^2 - 0.4688 d_j^2 - 0.1062 Q^2 \quad (7)$$

The coded factors equation can be used to predict the response for given levels of each factor. By default, the high levels of the factors are coded as +1, and the low levels are coded as -1. The coded equation helps identify the relative impact of the factors by comparing the factor coefficients.

The actual quadratic Equation for modeling

For smaller bucket size, $\emptyset_b = 0.67$

$$\delta_b)_{0.67} = 7.46765 - 5.55112E^{-16}\theta_j + 0.1750 d_j + 2.1750 Q - 0.3875\theta_j d_j - 0.050 d_j Q - 3.11875\theta_j^2 - 0.468750 d_j^2 - 0.106250 Q^2 \quad (8)$$

For larger bucket size, $\emptyset_b = 0.87$

$$\delta_b)_{0.87} = 6.83235 + 0.51250\theta_j - 0.66250d_j + 1.1250Q - 0.38750\theta_j d_j - 0.500\theta_j Q - 0.0500 d_j Q - 3.11875\theta_j^2 - 0.468750 d_j^2 - 0.106250 Q^2 \quad (9)$$

The above equations (8) and (9) are used to predict the bucket displacement of both the buckets used in the present study. The responses achieved with various combinations are mentioned in Fig. 7 below.

As the analysis software suggests, the model comparison is presented in Annexure A3. The quadratic model has acceptable values of statistical parameters like model p-value Adjusted R^2 and Predicted R^2. The fit statistics suggest how the observations match and fit the standard equations for better predictability. The Predicted R^2 of 0.8311 is in reasonable agreement with the Adjusted R^2 of 0.9279; i.e., the difference is less than 0.2. Adequate precision measures the signal-to-noise ratio. A ratio greater than 4 is desirable. The ratio of 19.5988 indicates an adequate signal. This model can be used to navigate the design space. The ANOVA for the quadratic model is depicted in Table 5 below. The R^2 and adjusted R^2 values should be at least 0.8 (or 80%) for a well-fitted model. In the present case, the R^2 and adjusted R^2 values exceeded 0.8, indicating that the constructed regression model effectively describes the behavior of the evaluated response variable. Annexure A4 shows the fit statics for bucket deflection. The adjusted R^2 (0.9279) should always be less than or equal to R^2 (0.9563). The prediction error sum of squares (PRESS) and coefficient of variation (CV) in the present study is above 4 and less than 10%, respectively, for the trueness of the test results.

Table 5: ANOVA for the bucket displacement BBD

Source	SoS	df	M.S	F-value	p-value
Model	146.56	13	11.27	33.68	<0.0001
Angle of jet (θ_j)	1.05	1	1.05	3.14	0.0917
Jet diameter (d_j)	0.9506	1	0.9506	2.84	0.1075
Flow rate (Q)	43.56	1	43.56	130.14	<0.0001
Bucket size ratio ($\emptyset_b$)	3.43	1	3.43	10.25	0.0045
$\boldsymbol{\theta_j \times d_j}$	1.20	1	1.20	3.59	0.0727
$\boldsymbol{\theta_j \times Q}$	2.00	1	2.00	5.98	0.0239
$\boldsymbol{\theta_j \times \emptyset_b}$	1.05	1	1.05	3.14	0.0917
$\boldsymbol{d_j \times Q}$	0.0200	1	0.0200	0.0598	0.8094
$\boldsymbol{d_j \times \emptyset_b}$	2.81	1	2..81	8.38	0.0090
$\boldsymbol{Q \times \emptyset_b}$	4.41	1	4.41	13.18	0.0017
$\boldsymbol{\theta_j^2}$	81.91	1	81.91	244.71	<0.0001
$\boldsymbol{d_j^2}$	1.85	1	1.85	5.53	0.0291
$\boldsymbol{Q^2}$	0.0951	1	0.0951	0.2840	0.6000

The statistical significance of the model is shown by the substantial impact of at least one component on bucket displacement. Bucket displacement is significantly influenced by the flow rate, with a p-value less than 0.0001 for both the jet angle and flow rate, indicating their significant impact. The bucket size ratio ($\emptyset_b$) also significantly affects displacement. Although jet diameter and angle are not statistically significant individually, they may still be important for the overall model. The Model F-value of 33.68 implies the model is significant, with only a 0.01% chance that an F-value this large could occur due to noise. P-values less than 0.0500 indicate significant model terms, including $\theta_j \times Q$, $d_j \times \emptyset_b$, $Q \times \emptyset_b$, θ_j^2, d_j^2, Q , and $\emptyset_b$. Model terms with p-values greater than 0.1000 are not considered statistically significant. Reducing inconsequential model terms (while maintaining hierarchy) could improve the model.

Fig. 7 illustrates the relationship between bucket displacement and jet diameter, jet angle, and flow rate for the 0.67 bucket size ratio. The 3D graphs plot the combination of any two variables, with the third constant showing a three-dimensional surface plot of the interaction between these parameters. The green mesh compares the model's predicted values and actual data points. The contour plot suggests that the jet angle's effect is maximized when the jet strikes the bucket normally. The 8 mm and 12 mm jet diameters are less effective than the 10 mm ones. For $\emptyset_b$ = 0.67, displacement increases with nozzle angle and diameter changes.

In Fig. 7, the top-right graph, the y-axis represents the angle of the jet (in degrees), while the x-axis shows the jet diameter (m). In the middle-right graph, the y-axis again represents the angle of the jet (in degrees), with the x-axis displaying the flow rate (in m^3/sec). In the bottom-right graph, the y-axis corresponds to the jet diameter (m), and the x-axis indicates the flow rate (in m^3/sec). The contour lines show the relationship between nozzle diameter and flow rate for $\emptyset_b$ = 0.67. Non-parallel lines indicate interaction between variables affecting bucket displacement, with larger nozzle diameters resulting in greater displacement. The relationship appears non-linear, with a steeper increase at higher nozzle diameters. Understanding this correlation is crucial for optimizing nozzle design to reduce bucket displacement and improve turbine efficiency. Contour plots also illustrate the relationship between bucket displacement (in mm) and various parameters, with different color gradients indicating displacement levels.

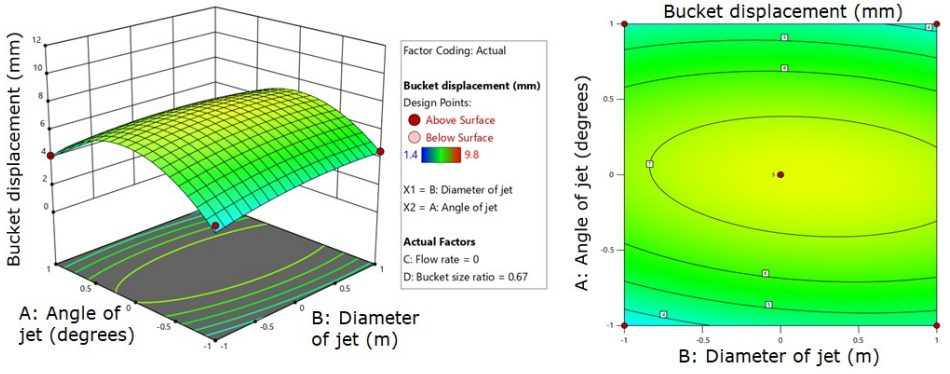

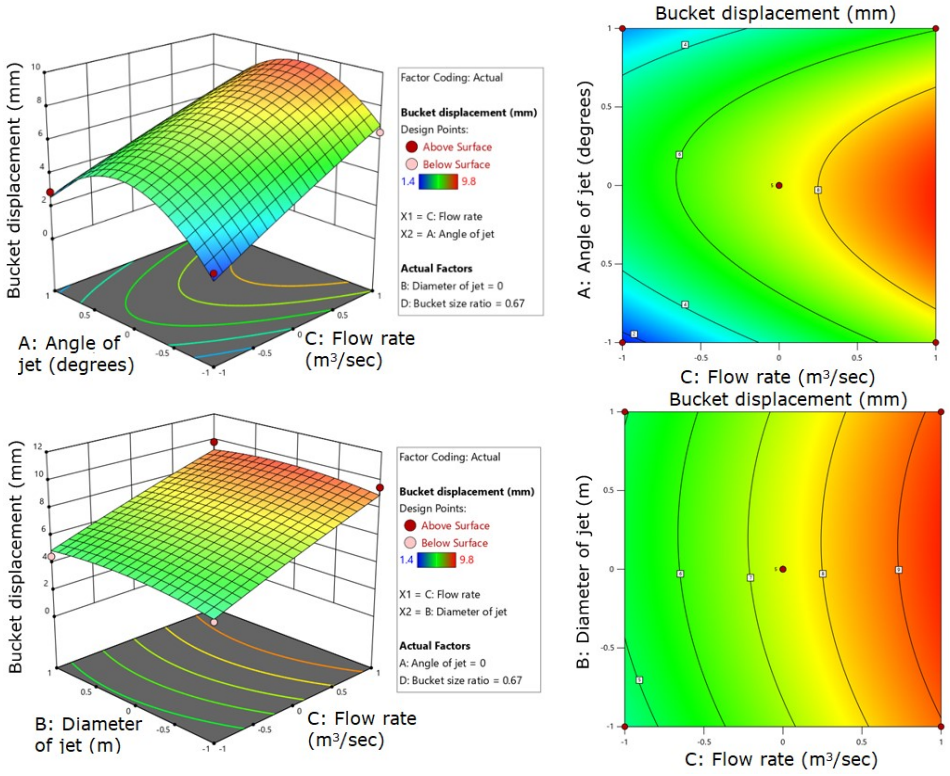

Figure 7: The model graph for the 3-D response surface obtained for bucket size ratio 0.67

The bucket displacement reduces as the nozzle angle increases from -1 to 1 (arbitrary units scaled for the plot). This suggests that the turbine buckets displaced less at increasing nozzle angles. The connection was non-linear, with a notable decrease in displacement as the nozzle angle rose, especially at higher flow rates. The contour lines at the plot's base highlight the relationship between flow rate and nozzle angle.

The contour lines that are not parallel indicate a noteworthy interaction impact between the two variables and bucket displacement. The nozzle angle predominantly affects displacement only at lower flow rates. Increasing the nozzle angle significantly reduces displacement at higher flow rates. The data show that bigger nozzle angles significantly reduce bucket displacement, particularly at higher flow rates. These observations help improve impulse turbine performance and structural integrity in small hydro applications by fine-tuning the design and operating parameters.

Optimum conditions for maximum bucket deflection

The optimal solution derived using Response Surface Methodology (RSM) with Box-Behnken Design (BBD) for the current study is illustrated in Fig. 8. The desirability ramp is graphically represented between the coded ranges (Minimum and Maximum). The red ball on the desirability ramp signifies the optimum value among the independent variables influencing bucket displacement. The parameters selected in this study significantly impact bucket displacement, with flow rate being the most influential. The jet incidence angle is ideally normal for Pelton turbine buckets, whereas for Turgo turbines, the jet striking angle is crucial.

In the present study, it has been found that the larger bucket ratio contributes to the maximum bucket displacement. As a categorical factor, the coded values for bucket sizes 0.67 and 0.87 are 1 and 2, respectively. The RSM resulted in the values of the numerical factors, such as the angle of the nozzle (θ_j), diameter of nozzle (d_j) and flow rate (Q) equals -0.000673316, -0.408509, and -0.320019, respectively, in terms of coded values. The red dot on the optimality ramp indicates the optimum value of coded parameters. The range of bucket displacement for the present study is between 1.4 to 9.8 mm. The corresponding response value for bucket displacement was a 0.87 bucket ratio of 6.64677 mm. The desirability value close to 1 indicates that the settings are achieving favorable results for all the responses. The larger size has a higher torque arm than the smaller bucket size ratio, contributing more torque. The angle of the nozzle with normal jet incidence has been more effective. The experimental graphs support and are also shown with RSM in each case.

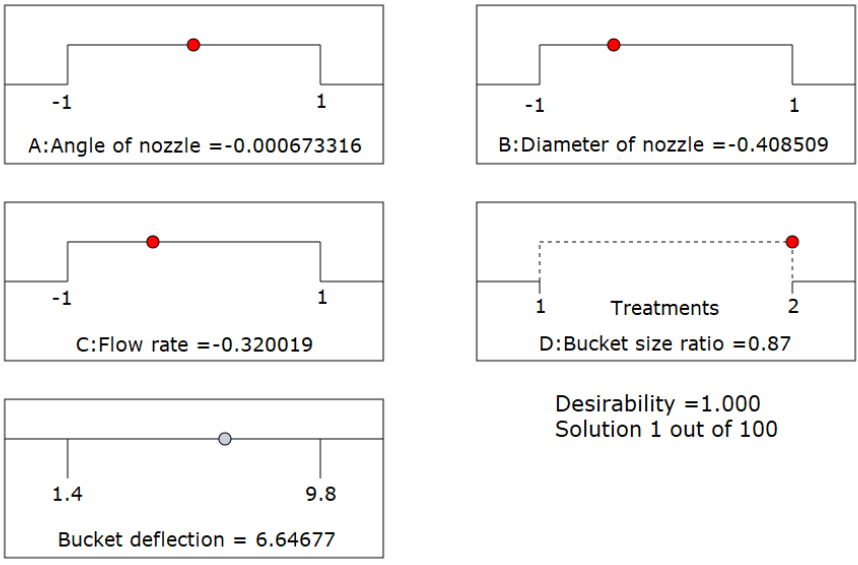

Figure 8: Desirability ramp for the optimum solution

The values corresponding to optimality are decoded and mentioned in Table 6. The optimal values for the input operating parameters in the present study yield the maximum bucket deflection for a bucket ratio of 0.87. The jet diameter for the optimum condition is 8.6 mm, which can be taken as 8 mm from the available nozzle diameters. The flow rate was found to be 0.0001156 m^3/s upon decoding.

Table 6: Optimum values for input parameters and corresponding response

Sr. No.	Bucket ratio ($\emptyset_b$)	Angle of jet (θ_j), degrees	Jet diameter (d_j), mm	Flow rate (Q), m^3/s	Bucket displacement (δ_b), mm	Goal
1	0.87	90	8.6	0.0001156	6.64677	Maximization

Table 7 juxtaposes the investigations conducted by various researchers to optimize parameters for attaining maximum efficiency. These studies have focused on metallic bucket materials and Turgo turbine runners. However, the present study diverges by utilizing different materials and runners, thereby identifying a research gap beyond the operating parameters. The results obtained in this study for optimized jet diameter, angle, and flow rate align with previous research, corroborating the findings.

Table 7: Comparison between the present study and previous work

Sr. No.	Author/s	Parameters considered	Type of work carried out	Conclusions relevant to the present study
1	Alomar et al., 2022	Pelton turbine runner, Aluminium material buckets, head =9.5 m, nozzle diameter= 9.5-12.5 mm (4 nos. in equal steps), Number of nozzles=1	Experimental	An increase in jet diameter reduces the head, and an increase in flow rate increases turbine efficiency.
2		Turgo turbine runner, 3-D printed buckets of PLA, head = 3 m, nozzle diameter= 8,9 and 10 mm, Number of nozzles=1	Experimental	A lower angle of jet striking yields maximum efficiency
3	Alnakhlani et al.2015	Pelton turbine runner, head=6.5=15.5 m, Number of nozzles=1	Experimental	An increase in bucket size and jet incidence angle increases the turbine efficiency.
4	Gallego et al., 2021	Turgo turbine runner, SS 304 buckets, head = 42 m, nozzle diameter= 10,15 and 20 mm, Number of nozzles =2	Experimental and RSM with BBD model	The nozzle diameter has a considerable effect on turbine efficiency

5	Gaiser et al., 2016	Turgo turbine runner, SS 304 buckets, head =35 m, nozzle diameter= 7.125, 12.85, and 18.59 mm, Number of nozzles=1	Experimental and RSM with CCD model	The nozzle diameter, jet inlet angle, number of blades, and blade speed were found effective compared to the jet striking location and blade orientation angle.
6	Williamson et al., 2013	Turgo turbine runner, head = 0.5 – 3.5 m, nozzle diameter=15-35 mm (5 nos. in equal steps)	Experimental and Design of Experiments (DOE)	The decreased head and the increased jet diameter diminish the turbine efficiency.
7	Present study	Pelton turbine bucket,3-D printed buckets of PLA, head = 7 m, nozzle diameter= 8,10, and 12 mm, Number of nozzles=1	Experimental and RSM with BBD model	An increase in flow rate affects the bucket displacement most; normal jet incidence causes maximum displacement.

The outcomes derived from the RSM model are juxtaposed with the empirical data delineated in Table 8 to ascertain the optimal conditions for the specified parameters. The validation test reveals minimal observed discrepancy (0.79%) between the actual and forecasted bucket displacement, indicating a strong concordance between the designed model and the experimental findings.

Table 8: Comparison of bucket displacement (δ_b) between experimental and RSM results

Bucket size	**Bucket displacement ($\boldsymbol{\delta_b}$)**, mm		
	Experimental results	RSM results	Error (%)
Larger bucket, $\emptyset_{\boldsymbol{b}}$ = 0.87 Width (B) =76 mm	6.69995	6.64677	0.79

An accuracy error below 5% for the RSM validation is deemed satisfactory. Consequently, the experiment and the RSM model strongly correlate with predicting displacement with a 0.87 bucket ratio. This study has established a robust foundation for utilizing PLA as a viable bucket material in small hydro applications.

CONCLUSIONS

In this study, experimental investigations were carried out using the widely adopted Response Surface Methodology (RSM) with Box-Behnken Design (BBD) to model a second-order response surface. The independent variables include numerical and categorical factors (bucket size ratio). The numerical factors were set at three equally spaced levels, coded as d_j,θ_j, and Q. The following conclusions are obtained by maximizing bucket displacement based on optimizing selected independent variables.

It has been found from the literature review that the optimization for impulse turbine bucket design, bucket material, runner diameter, jet ratio, varying flow, and head has been studied so far. Still, the effect of bucket production type, sustainable bucket material, jet angle, and size ratio has not been identified and studied extensively for the low-head application of the Pelton turbine bucket. A substantial effect of the increase in bucket size ratio was found on displacement. With a 30% increase in bucket size ratio, the force and subsequent bucket displacement have enhanced. The volume of water, less likely water diffusion, and the uplift of the moment arm due to size caused increased displacement in the larger bucket (0.87). The bucket with a size ratio of 0.67 experienced significant jet diffusion. Post-strike, the unexpanded bifurcated jet flows adversely affected displacement, especially at jet diameters exceeding 10 mm. Thus, the bucket size ratio of 0.87 is more effective than 0.67. The increase in jet diameter has a diminishing effect on bucket displacement. It was also observed to deteriorate even when struck with something other than normal in the bucket. The increased jet diameter was found to be effective at up to 10 mm for both buckets for the range of experiments.

The experimental observations have confirmed that the nozzle angle of 90° was more effective for bucket displacement than the rest. It was observed that larger diameter jets incurred hydraulic losses due to jet spreading, reducing the kinetic energy reaching the bucket surface. NOVA analysis has shown that the bucket displacement is sensitive to flow rate as the p-value is less than 0.0001 and the jet angle is next to it. In the present study, the effect of jet diameter is reported very little on bucket displacement. The selected quadratic model is suitable for predicting bucket displacement of low-weight material.

The optimal values are a nozzle angle of 90°, a jet diameter of 8.82 mm, and a flow rate of 0.0001156 m^3/s. Statistical analysis has shown that a jet diameter over 8.82 mm affects efficiency. Therefore, the next available 10 mm exit diameter nozzle is suitable. The developed RSM model results were compared with experimental results to validate optimum values operating parameters. The error of 0.79% has shown that the predicted and experimented bucket displacement values are in good agreement after the validation test. The present study was conducted to provide bucket design information for researchers, small-scale hydroelectric manufacturers, and individual developers. This information provides cost-effective, high-efficiency Pelton turbine buckets optimized for specific small-hydro sites. This could be critical in fluid dynamics, mechanical systems, or hydraulic structures, where precise displacement control is crucial.

Declaration of competing interest

The authors declare that they have no known competing financial interests or personal relationships that could have appeared to influence the work reported in this paper.

Acknowledgment

The authors gratefully acknowledge the extended technical support from "MET- HEAT SERVICES," a material testing laboratory in Vadodara, Gujarat, for providing surface roughness certification for manufactured buckets in time.

REFERENCES

ADANTA D., FEBRIANSYAH D. (2020). Feasibility analysis of a pico-scale Turgo turbine bucket using coconut shell spoons for electricity generation in remote areas in Indonesia, Journal of Advanced Research in Fluid Mechanics and Thermal Sciences, Vol. 69, Issue 1, pp. 85–97.

ADANTA D., PUTA N.S., VOHRA H. (2018). Cutout types analysis on Pico hydro Pelton turbine, International Journal on Advanced Science, Engineering and Information Technology, Vol. 8, Issue 5, pp. 2024–2030.

ALNAKHLANI M.M., MUKHTAR, HIMAWANTO D.A., ALKURTEHI A., DANARDONO D. (2015). Effect of the bucket and nozzle dimension on the performance of a Pelton water turbine, Modern Applied Science, Vol. 9, Issue 1, pp. 25-33.

ALOMAR O.R., ABD M.H., SALIH M.M.M., ALI A.F. (2022). Performance analysis of Pelton turbine under different operating conditions: An experimental study, Ain Shams Engineering Journal, Vol. 13, Issue 4, Paper ID 101684.

AMARA L., ACHOUR B., BERREKSI A. (2013). Finite volumes numerical approach for the calculation of the dynamic response of equilibrium chimneys, Larhyss Journal, No 14, pp. 7-19. (In French)

AMARA L., BERREKSI A., ACHOUR B. (2016). Application of the finite volume method to the computation of water hammer protection, Larhyss Journal, No 28, pp. 303-317. (In French)

AMARA L., ACHOUR B. (2020). Discharge of "coefficient of shaft spillway under small heads" by Gouryev A.P., Brakeni A., Beglarova E.C, Larhyss journal, No 43, pp. 7-11.

AMBALIYA SANJAY D., DHIMAN VIJAY D., MISTRY MANISH K. (2024). Experimental analysis and parametric investigation of water electrolysis process for hydrogen gas production, Larhyss Journal, No 59, pp. 85-100.

AROUA N. (2020). Flood risk reduction strategy in Algiers a brief modern history (XVIthC -XIXthC), Larhyss Journal, No 43, pp. 73-89.

BELLOUFI Y., BRIMA A., ATMANI R., MOUMMI N., AISSAOUI F. (2016). Theoretical and experimental study of air refresh by a geothermal heat exchanger air/ ground, Larhyss Journal, No 25, pp. 121-137. (In French)

BENZON D.S., AGGIDIS G.A., ANAGNOSTOPOULOS J.S. (2016). Development of the Turgo Impulse turbine: Past and present, Applied Energy, No 166, pp. 1–18.

BETANCOUR J., ROMERO-MENCO F., VELÁSQUEZ L., RUBIO-CLEMENTE A., CHICA E. (2023). Design and optimization of a runner for a gravitational vortex turbine using the response surface methodology and experimental tests, Renewable Energy, No 210, pp. 306–320.

BHATTARAI S., DAHAL K., VICHARE P., MISHRA B. (2018). CFD-Based Stochastic Optimization of Pelton Turbine Bucket in Stationery Condition, Proceedings of 2018 9th International Conference on Mechanical and Aerospace Engineering, ICMAE 2018, July 10, pp. 53–57.

BOUBOU-BOUZIANI N. (2015). The energy challenge: the other aspect of the water issue, Larhyss Journal, No 22, pp. 109-122. (In French)

BUDIARSO D.F., FEBRIANSYAH D., ADANTA D. (2020). The effect of wheel and nozzle diameter ratio on the performance of a Turgo turbine with Pico scale, Energy Reports, No 6, pp. 601–605.

BUDIARSO D.F., WARJITO, NAUFAL LUBIS M., ADANTA D. (2019). Performance of a low-cost spoon-based Turgo turbine for Pico hydro installation, Energy Procedia, No 156, pp. 447–451.

BOUVANT M., BETANCOUR J., VELÁSQUEZ L., RUBIO-CLEMENTE A., CHICA E. (2021). Design optimization of an Archimedes screw turbine for hydrokinetic applications using the response surface methodology, Renewable Energy, No 172, pp. 941–954.

BOX G.E.P., HUNTER J.S., HUNTER W.G. (2005). Statistics for Experimenters: Design, Innovation, and Discovery, Book, John Wiley and Sons Ltd., 2nd Edition, USA.

CHAOUI S., HOUICHI L., TEBBI F.Z. (2016). Numerical simulation using characteristics method of pressurized transient flow in a water supply gravity pipe, Larhyss Journal, No 25, pp. 83-99. (In French)

CHITRAKAR S., SOLEMSLIE B.W., NEOPANE H.P., DAHLHAUG O.G. (2020). Review on numerical techniques applied in impulse hydro turbines, Renewable Energy, No 159, pp. 843–859.

DEBBACHE M., DERFOUF S. (2018). Analysis of the induction effect on the performance of wind turbine, Larhyss Journal, No 33, pp. 25-39.

EBHOTA W.S., INAMBAO F.L. (2019). Smart Design and Development of a Small Hydropower System and Exploitation of Locally Sourced Material for Pelton Turbine Bucket Production, Iranian Journal of Science and Technology, Transactions of Mechanical Engineering, Vol. 43, Issue 2, pp. 291–314.

ELGAMMI M., HAMAD A.A. (2022). A feasibility study of operating a low static pressure head micro-Pelton turbine based on water hammer phenomenon, Renewable Energy, No 195, pp. 1–16.

FAYE C. (2016). Management of water resources in the local of Ndondol: study of community management of water resources and water use conflicts in Mbomboye villages (Senegal), Larhyss Journal, No 25, pp. 219-240. (In French)

GAISER K., ERICKSON P., STROEVE P., DELPLANQUE J.P. (2016). An experimental investigation of design parameters for pico-hydro Turgo turbines using a response surface methodology, Renewable Energy, No 85, pp. 406–418.

GALLEGO E., RUBIO-CLEMENTE A., PINEDA J., VELÁSQUEZ L., CHICA E. (2021). Experimental analysis on the performance of a pico-hydro Turgo turbine. Journal of King Saud University, Engineering Sciences, Vol. 33, Issue 4, pp. 266–275.

GORAN R., JELISAVKA B. (2016). Possibility of use of water in the economy of Montenegro, Larhyss Journal, No 25, pp. 7-30.

GOURYEV A.P., BRAKENI A., BEGLAROVA E.C. (2020). Discharge coefficient of shaft spillway under small heads, Larhyss Journal, No 42, pp. 23-39.

GUERRA J., VELÁSQUEZ L., RUBIO-CLEMENTE A., JARAMILLO L., CHICA E. (2024). Design and optimization of a siphon turbine using the response surface methodology, Results in Engineering, No 22, Paper ID 102241.

GUPTA V., PRASAD V., KHARE R. (2016). Effect of jet length on the performance of Pelton turbine: Distance between nozzle exit and runner, Journal of Engineering and Applied Sciences, Vol. 11, Issue 19, pp. 11487–11494.

HAFNAOUI M.A., MADI M., BEN SAID M., BENMALEK A. (2022). Floods in El Bayadh city: causes and factors, Larhyss Journal, No 51, pp. 97-113.

HAFNAOUI M.A., BOULTIF M., DABANLI I. (2023). Floods in Algeria: analyzes and statistics, Larhyss Journal, No 56, pp. 351-369.

ISHOLA F.A., AZETA J., AGBI G., OLATUNJI O.O., OYAWALE F. (2019). Simulation for material selection for a Pico Pelton turbine's wheel and buckets, Procedia Manufacturing, No 35, pp. 1172–1177.

JUNG I.H., KIM Y.S., SHIN D.H., CHUNG J.T., SHIN Y. (2019). Influence of spear needle eccentricity on jet quality in micro-Pelton turbine for power generation, Energy, No 175, pp. 58–65.

KHOLIFAH N., SETYAWAN A.C., WIJAYANTO D.S., WIDIASTUTI I., SAPUTRO H. (2018). Performance of Pelton Turbine for Hydroelectric Generation in Varying Design Parameters, IOP Conference Series: Materials Science and Engineering, Vol. 288, Issue 1, Paper ID 012108.

KIM J.W., JO I.C., PARK J.H., SHIN Y., CHUNG J.T. (2017). Theoretical method of selecting number of buckets for the design and verification of a Pelton turbine, Journal of Hydraulic Research, Vol. 55, Issue 5, pp. 695–705.

LAJQI S., BRESA Q., BRESA A., DOÇI I., ĐURIN B. (2021). Design, implementation, and analysis of the overall performance of a micro hydro Turgo turbine, Journal of Thermal Engineering, Vol. 7, Issue 4. pp. 806-822.

LONG A., MOKHTAR M., HALIM S., AHMED F. (2023). Fostering inclusive watershed management through multihelix engagement model on micro hydropower electrification in Sabah, Malaysia, Larhyss Journal, No 56, pp. 7-24.

MEHTA D., ACHOUR B., PASTAGIA J., AZAMATHULLA H., VERMA S. (2023). Review of reservoir operation, Larhyss Journal, No 56, pp. 193-214.

NEDELCU D., COJOCARU V., AVASILOAIE R.C. (2021). Numerical investigation of Nozzle jet flow in a Pelton microturbine, Machines, Vol. 9, Issue 8, Paper ID 158.

PERRIG A., AVELLAN F., KUENY J.L., FARHAT M., PARKINSON E. (2006). Flow in a Pelton turbine bucket: Numerical and experimental investigations, Journal of Fluids Engineering, Transactions of the American Society of Mechanical Engineers (ASME), Vol. 128, Issue 2, pp. 350–358.

RAYMOND M.H., DOUGLAS M.C., CHRISTINE A.C. (2016). Response Surface Methodology: Process and Product Optimization Using Designed Experiments, Book of Wiley Series in Probability and Statistics, John Wiley and Sons Inc., 4th Edition, New Jersey, USA.

RENATA R.T., PEREIRA F.F.S., DA SILVA T.B.G., CASTRO E.R., SAAD J.C.C. (2020). The performance of explicit formulas for determining the Darcy Weisbach friction factor, Engenharia Agricola, Vol. 40, Issue 2, pp. 258–265.

REMINI B. (2023). Flash floods in Algeria, Larhyss Journal, No 56, pp. 267-307.

SALAH B., KETTAB A, MASSOUH F. (2003). Water hammer in a buried branched network in backflow, Larhyss Journal, No 2, pp. 55-68. (In French)

SEMLITSCH B. (2024). Effect of inflow disturbances in Pelton turbine distributor lines on the water jet quality, International Journal of Multiphase Flow, No 174, Paper ID 104786.

SHAIKH A.F., BHIRUD Y.L., MORE S.B., PAWAR A.D., VAIDYA O.V. (2024). Comparative analysis of optimization algorithms for reservoir operations: a case study on Ukai dam, Larhyss Journal, No 58, pp. 179-196.

SOE M.M., WAR W., SWE M., THU A.M., KO LATT A. (2019). Effect of Jet Angle on the Performance of a Turgo Turbine, Iconic Research And Engineering Journals, Vol. 2, Issue 12, pp. 203–207.

STAUBLI T., WEIBEL P., BISSEL C. (2009). Jet quality and Pelton efficiency, Proceedings of the International Conference HYDRO 2009, Lyon, France, 26-28 October, pp. 26-28

SUYESH B., PARAG V., KESHAV D., AHMED A.M., ABDUL-GHANI O. (2019). Novel trends in modelling techniques of Pelton Turbine bucket for increased renewable energy production, Renewable and Sustainable Energy Reviews, No 112, pp. 87–101.

VELÁSQUEZ L., POSADA A., CHICA E. (2022). Optimization of the basin and inlet channel of a gravitational water vortex hydraulic turbine using the response surface methodology, Renewable Energy, No 187, pp. 508–521.

VERMA S., SAHU R.T., PRASAD A.D., VERMA M.K. (2023). Reservoir operation optimization using ant colony optimization a case study of Mahanadi reservoir project complex Chhattisgarh – India, Larhyss Journal, No 53, pp. 73-93.

VESSAZ C., JAHANBAKHSH E., AVELLAN F. (2015). Flow simulation of jet deviation by rotating Pelton buckets using finite volume particle method, Journal of Fluids Engineering, Transactions of the American Society of Mechanical Engineers (ASME), Vol. 137, Issue 7, Paper ID 074501.

WARJITO ADANTA D., BUDIARSO, PRAKOSO A.P. (2018). The effect of bucket number on breastshot waterwheel performance, IOP Conference Series: Earth and Environmental Science, Vol. 105, Issue 1, Paper ID 012031.

WILLIAMSON S.J., STARK B.H., BOOKER J.D. (2013). Performance of a low-head pico-hydro Turgo turbine, Applied Energy, No 102, pp. 1114–1126.

ZAMANI M., SHAFAGHAT R., KHARKESHI B.A. (2023). Experimental Investigation on the Effect of Flow Rate and Load on the Hydrodynamic Behavior and Performance of an Archimedes Screw Turbine, International Journal of Engineering, Transactions A: Basics, Vol. 36, Issue 4, pp. 733–745.

ZEGAIT R., PIZZO H.S. (2023). Flood control reservoir using VBA simulation case of Idles basin in southern Algeria, Larhyss Journal, No 53, pp. 41-60.

ŽIDONIS A., AGGIDIS G.A. (2016). Pelton turbine: Identifying the optimum number of buckets using CFD, Journal of Hydrodynamics, Vol. 28, Issue 1, pp. 75–83.

Annexure A1: Small bucket ($\emptyset_b$ = 0.67) design specification

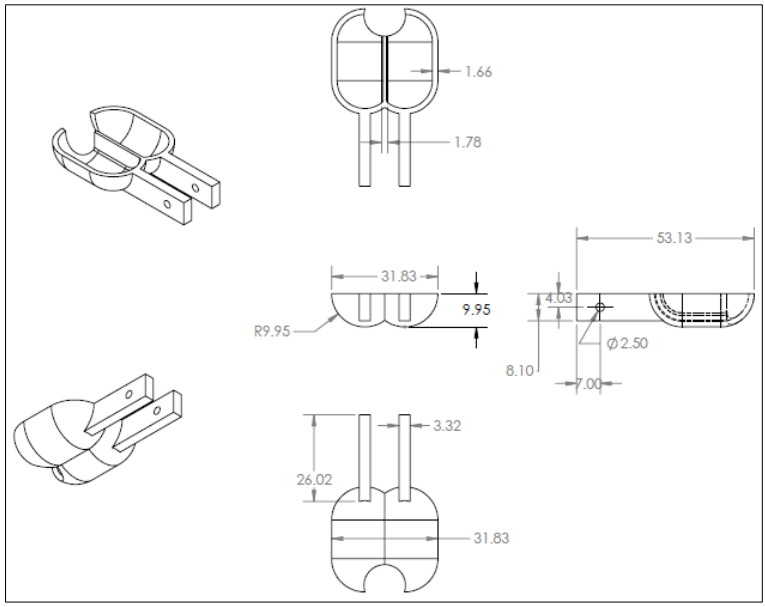

Annexure A2: Large bucket ($\emptyset_b$ = 0.87) design specification

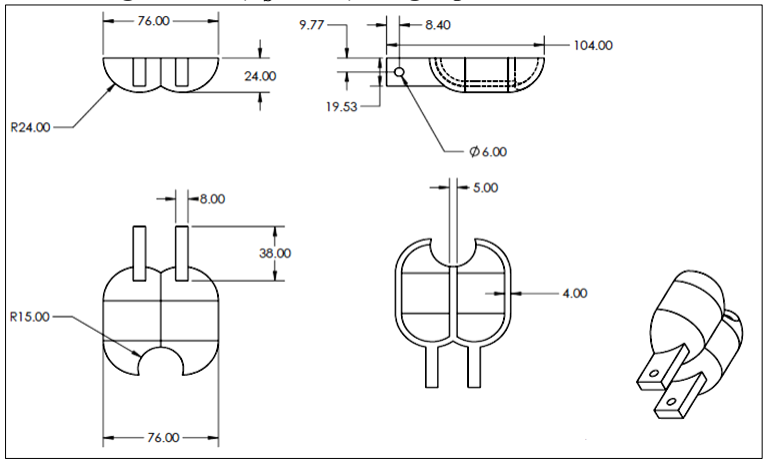

Annexure A3: Model summary statistics

Source	Std. Dev.	R^2	Adjusted R^2	Predicted R^2	PRESS	-----
Linear	1.90	0.3197	0.2258	0.0554	144.76	-----
2FI	2.01	0.3946	0.1314	-0.4784	226.57	
Quadratic	0.5786	0.9563	0.9279	0.8311	25.89	Suggested
Cubic	0.3668	0.9903	0.9710	0.4975	77.00	Aliased

Annexure A4: ANOVA Fit value for experimental and predicted (Quadratic model)

Std. Dev.	0.5786	R^2	0.9563
Mean	5.41	Adjusted R^2	0.9279
C.V. %	9.74	Predicted R^2	0.8311
PRESS	25.89	Adeq Precision	20.8022